Supplementary Material for Kovaleva et al. AM-15-85236

Planar microstructures in zircon

In the current context the term "planar microstructures" comprises all groups of different planar features described for zircon, including planar deformation features (PDFs), planar fractures (PFs), microcleavage, shock twins, phase transition along the certain planes and planar deformation bands (PDBs).

Planar deformation features (PDFs) in zircon, as defined by Erickson et al. (2013a), are shock-induced planar lamellae that crosscut the zircon crystal lattice along specific crystallographic planes and are filled with amorphous material or so-called "diaplectic glass"; or represent lattice domains with a high defect density (Leroux et al., 1999; Timms et al., 2012b; Grange et al. 2013). Planar lamellae filled with amorphous material have not been yet documented in natural terrestrial zircon samples (Erickson et al. 2013a) and the phenomena defined as PDFs in natural terrestrial zircon are usually planar fractures (e.g. Bohor et al. 1993; Corfu et al. 2003). But Timms et al. (2012b, fig. 8) and Grange et al. (2013, fig. 12) describe true PDFs in lunar zircon. These are identified by optical microscopy, in EBSD maps representing planes of low EBSD pattern quality, and in rare cases as dark lines in CL images. The crystallographically-controlled thin (<200 nm) layers of amorphous material or "diaplectic glass" were produced experimentally by Leroux et al. (1999). PDFs occupy {320} and {110} (Leroux et al., 1999) and also {112} and {001} (Timms et al. 2012b) crystallographic planes in zircon and result from 40 GPa shock pressure (Leroux et al. 1999), being considered to be indicative of shock pressure.

Planar fractures (PFs) or parallel and closely-spaced open structures resembling cleavage, are well-known from terrestrial and lunar impactites (e.g. Bohor et al. 1993; Kamo et al. 1996; Kalleson et al. 2009; Cavosie et al. 2010; Moser et al. 2011; Erickson et al. 2013a, 2013b; Thomson et al. 2014). These shock-produced fractures are particularly noticeable in minerals such as quartz, garnet, monazite and zircon, which do not normally reveal any cleavage in most terrestrial tectonic settings (Timms et al. 2012b). PFs in zircon are usually detected by scanning electron microscopy (SEM) on etched surfaces (e.g. Bohor et al. 1993; Kamo et al. 1996; Erickson et al. 2013a, 2013b; Thomson et al. 2014), and are often visible in the transmitted or reflected light microscope (Corfu et al. 2003; Thomson et al. 2014). Representing open structures, PFs can be filled with other material, and become noticeable in CL-images tracing as bright or dark patterns decorated by voids and pores. PFs can offset growth zonation (e.g. Kalleson et al. 2009; Cavosie et al. 2010; Moser et al. 2011; Erickson et al. 2013a, 2013b; Thomson et al. 2014); some PFs cause crystal lattice rotations from 1 to 10° (Erickson et al. 2013a). PFs in natural zircon are most frequently parallel to the {100}, {001}, {112} and {011} planes (Cavosie et al. 2010; Erickson et al. 2013a; Leroux et al. 1999). In experimental samples they also occupy (201), (211), (221) and (111) planes (Leroux et al. 1999).

Apart from planar fractures, sets of roughly parallel non-planar or curviplanar fractures (CFs) are also considered to be associated with impact events (Cavosie et al. 2010; Moser et al. 2011; Timms et al. 2012b; Erickson et al. 2013a). They may be crystallographycally-controlled and may act as channels for impact melt (Moser et al. 2011; Erickson et al. 2013a).

Shock twins or microtwins are considered to be a characteristic feature of shock-deformed zircon grains (Leroux et al. 1999; Moser et al. 2011; Timms et al. 2012b; Erickson et al. 2013a, 2013b; Thomson et al. 2014). They were documented with EBSD mapping and TEM imaging and occupy {110} crystallographic planes with twin individuals rotated at 65° to the host lattice.

Reidite, the high-pressure shock induced polymorph of zircon with scheelite structure was documented with TEM occurring along {100} planes. Shock twins and reidite formation indicate shock pressure above 40 GPa (Leroux et al. 1999).

Planar deformation bands (PDBs) in zircon were described as planar portions of crystal lattice parallel to {100} planes, with few to hundreds of micrometers thickness showing misorientation up to 10° with respect to the host grain (Nemchin et al. 2009, Fig. 1; Timms et al. 2012b, Fig. 5). PDBs form two orthogonal sets crosscutting the initial growth zoning. They can be revealed only by orientation- and EBSD mapping. The most common misorientation axes for PDBs are <001>, and the geometry of dislocation glide system, therefore, is considered to be <100>{010}. This is characteristic not only for impact-related dislocations (Leroux et al. 1999; Timms et al. 2012b), but also a dominant glide system in tectonically deformed zircon grains (e.g. Reddy et al. 2007; Kaczmarek et al. 2011; Piazolo et al. 2012; Kovelava et al. 2014).

Otherwise oriented planar microstructures in zircon were produced during shock recovery experiments by Leroux et al. (1999). At shock pressure of 20 GPa planar fractures or microcleavage along {100} and sometimes {310} planes were formed. Multiple dislocations indicate that shock-related intense crystal-plastic deformation occurs. Sometimes shock-related dislocations are aligned in narrow "*micro-bands*", occupying glide planes {100}, which possibly could act as precursor for planar fractures.

However, shock-induced structures are not the only planar structures known in zircon. Some parallel parting has been observed in zircons from upper crustal xenoliths (Rudnick and Williams, 1987; Chen et al., 1994) and interpreted to form due to rapid decompression (Rudnick and Williams, 1987). Kresten et al. (1975) report on perfect partings or cleavages extending in several directions in kimberlitic zircon. Although such structures never appear to be perfectly parallel, as shock-induced structures do.

ANALYTICAL METHODS AND DATA REPRESENTATION

Sample preparation

Zircon grains were examined in polished thin sections of rock chips and in grain separates embedded in epoxy resin. For the latter zircon grains were extracted from the host rock by the standard procedure involving rock crushing, sieving to the 300 µm size, density separation on a Wilfley table, in heavy liquids and with Frantz magnetic separator. All samples were mechanically polished with 0.25 µm diamond paste and subsequently chemically polished with alkaline colloidal silica solution on an active rotary head polishing machine for 4 hours. Samples were cleaned in ethanol and distilled water before carbon coating that was applied to establish electrical conductivity.

Scanning electron microscopy and cathodoluminescence (CL) imaging

All zircons were identified and characterized by backscattered-electron (BSE) and cathodoluminescence (CL) imaging in order to reveal the internal microstructures, using a FEI Inspect S scanning electron microscope equipped with a Gatan MonoCL system (Center of Earth Sciences, University of Vienna, Austria). Energy-dispersive X-ray spectrometry (EDS) was applied to identify the host phases. Imaging conditions were 10 kV accelerating voltage, CL-image resolution: 1500*1500 to 2500*2500 pixels using a dwell time of 80.0-150.0 ms and probe current/spot size 4.5-5.0.

Forward scattered electron (FSE) imaging and electron backscatter diffraction (EBSD) analysis

Zircon grains were examined for potential crystal-plastic deformation structures using orientation contrast images that were taken using a forescattered-electron detector (FSD) mounted on the EBSD-tube of a FEI Quanta 3D FEG instrument (Faculty of Geosciences, Geography and Astronomy at the University of Vienna, Austria). For FSE imaging the EBSD tube has been retracted by c. 5 mm in order to obtain maximum signal intensity on the FSD. After identification of the potentially deformed grains, EBSD orientation mapping was applied to selected zircon grains or grain domains. The FEI Quanta 3D FEG instrument is equipped with an EDAX Pegasus Apex 4 system consisting of a Digiview IV EBSD camera and an Apollo XV silicon drift detector for EDX analysis. EDX intensities and EBSD data were collected contemporaneously using the OIM data collection software v6.2.1. FSD settings and EBSD orientation mapping settings applied are discussed in details in Kovaleva et al. (2014). Orientation maps were obtained from beam scanning in hexagonal grid mode at step sizes of 0.1 – 0.2 micrometer.

Raw indexing for zircon grains is more than 99.99%. In some cases, after EBSD data collecting the maps were recalculated based on chemical composition of phases with the OIM v6.21 software.

All EBSD data are presented in the sample reference frames X-Z or Y-Z. The EBSD data are presented as EBSD pattern quality images, and as false color-coded misorientation maps, with colors showing the relative angular misorientation of each data point with respect to a user-selected single reference point within the grain. The reference point is indicated by a red marker in each EBSD map. The orientations of the crystallographic axes are plotted as lower hemisphere equal area projections and are color-coded according to the corresponding EBSD map. The EBSD maps and pole figures were produced using the EDAX OIM Analysis software v6.2.1. All FSE and EBSD maps as well as the pole figures are oriented with X (Y) positive up and Z positive left.

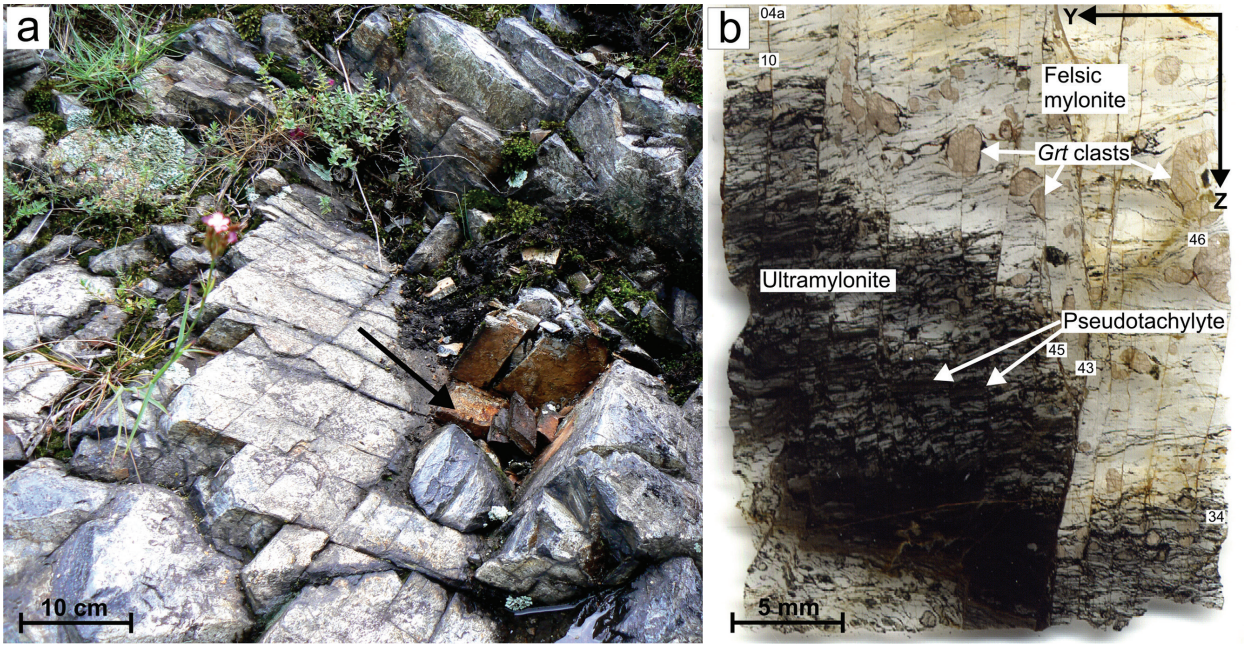

APPENDIX FIGURE 1. (**a**) Field photograph of the sampled outcrop, sampled site is indicated by arrow. (**b**) Plane-polarized transmitted light photograph of the thin section with shear zone (dark area). Grt = garnet. Axes show orientation of thin section in the sample reference frame. Labels with numbers are locations of the analyzed zircon grains.

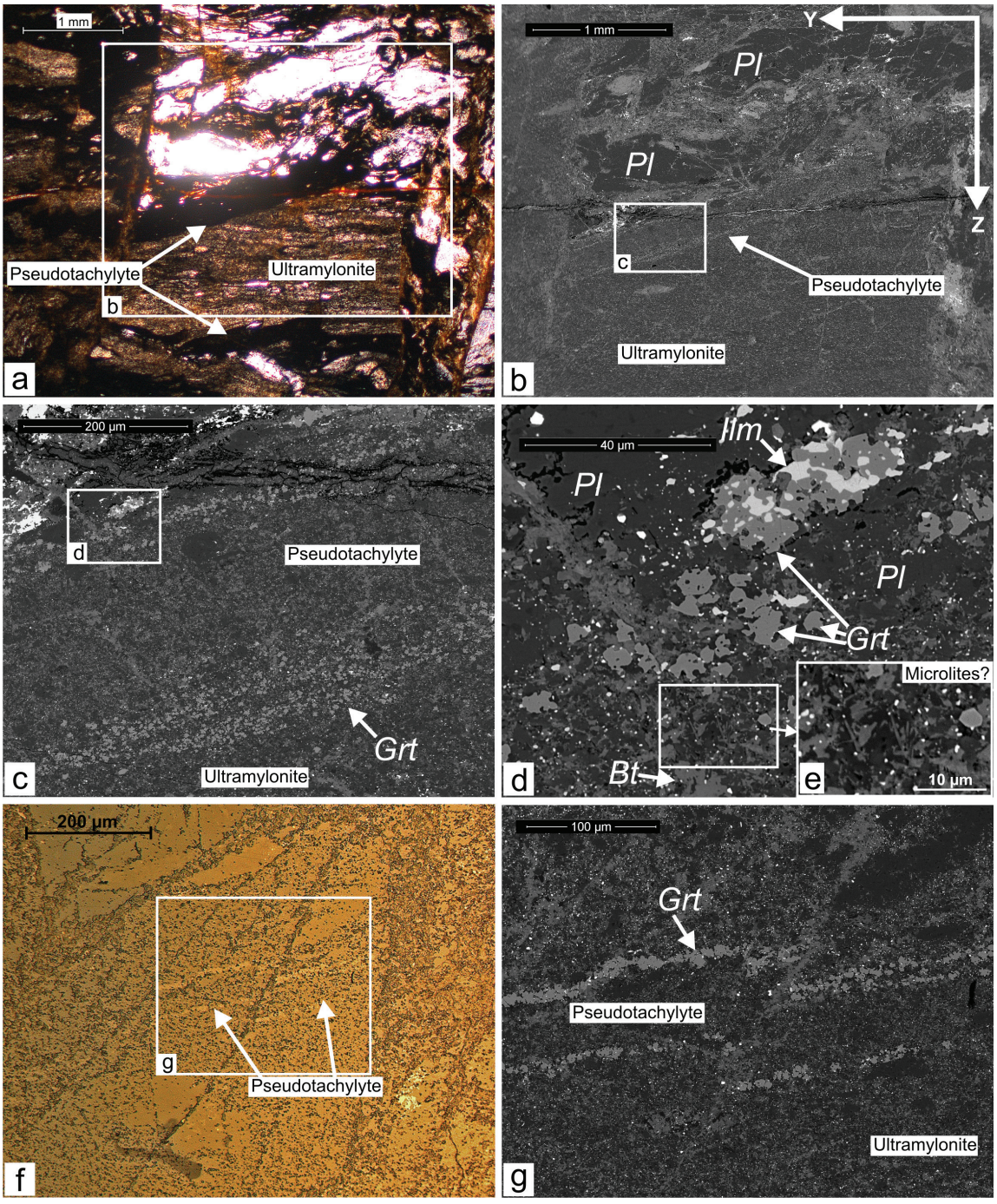

APPENDIX FIGURE 2. Pseudotachylyte veins (orientation as in Fig. 1b). Pl = plagioclase, Grt = garnet, Ilm = ilmenite, Bt = biotite. (**a**) Plane-polarized transmitted light photomicrograph, black veins are pseudotachylytes hosted by ultramylonite. (**b**) BSE image of the area marked in **a**. Pseudotachylyte vein with bright rim due to garnet enrichment in contact with ultramylonite. (**c**) BSE image of pseudotachylyte vein in detail. (**d**) BSE image of the rim of pseudotachylyte vein. (**e**) Enlarged area from **d** with needle-shaped fine grains, resembling microlites. (**f**) Reflected light photomicrograph. The pseudotachylyte vein has a garnet rim (bright), separating it from the host ultramylonite. (**g**) BSE image of the pseudotachylyte vein shown in **f**, offset by a fracture zone.

We also gained insight into geometrically necessary dislocation densities using Weighted Burgers Vector (WBV) calculations (Wheeler et al. 2009). Rectangular areas with WBV components were calculated over the EBSD maps with the MATLAB toolbox CrystalScape 1.3 based on the method described in Wheeler et al. (2009). For this goal the maps were transformed to a square

grid and the Euler angles were recalculated accordingly with the Channel software. The actual algorithm used by Channel to import .ang files produces a square grid of data points and reduces the number of data points by approximately $(\sqrt{3})/2$, which should involve some kind of interpolation to create the square grid. This may introduce errors – but the key point here is that in using the integral method to determine WBV, in which an integration path passes through many pixels, the effects of local errors are reduced and thus not compromise our interpretations. The rectangular areas, presented in this publication, are superimposed on the EBSD pattern quality maps with hexagonal grid, derived with EDAX OIM Analysis software, where deformation structures are better visible.

PETROGRAPHY

Felsic mylonites represent strongly restitic, highly dehydrated metasedimentary rocks. They contain garnet clasts ranging from 50 to 500 μm in size (Appendix Fig. 1b), which are surrounded by a fine-grained foliated matrix consisting of alternating plagioclase- and quartz-rich layers, with intercalated biotite-ilmenite layers. Accessory minerals are zircon and monazite.

Locally pseudotachylytes are visible macroscopically as concordant dark-gray 2-3 mm thick veins, fractured and offset by fractures. More often they are hosted by ultramylonites from which they are hard to distinguish. Ultramylonitic shear zones in the felsic mylonites appear as 1-2 cm thick dark rock portions extending parallel to the main foliation and limited by subvertical fractures (Appendix Fig. 1b). Shear zones contain pseudotachylyte veins concordant with the foliation, intensively folded and offset by fractures (Appendix Figs. 1b; 2a-b; 2f-g).

Both pseudotachylytes and ultramylonites mainly represent an ultra-fine-grained matrix composed of plagioclase, quartz, biotite and ilmenite, with minor amounts of garnet. Unlike the mylonitic portions of the rock, the ultramylonite contains much less garnet clasts, and does not reveal monomineralic bands. The foliation in ultramylonite is represented by variations in the biotite-content. Pseudotachylytes can be occasionally distinguished from surrounding ultramylonites in optical microscope as homogeneously black layers in plane-polarized light (Appendix Fig. 2a), but more often as layers with bright rims in reflected light (Appendix Fig. 2f) and BSE images (Appendix Figs. 2b-c, 2g).

Pseudotachylytes are often rimmed by single garnets and garnet aggregates of second generation (Appendix Fig. 2), which is different from host rock garnets. These garnet grains have a dendritic morphology, range from 5 to 40 μm in size, and contain multiple inclusions, mostly ilmenite (Appendix Fig. 2d) as described by Austrheim et al. (1996), Austrheim and Corfu (2009) and Pittarello et al. (2012). Garnets rimming pseudotachylyte are supposed to form due to late low-temperature (about 550°) crystallization of garnet from the melt (Pittarello et al. 2012). Sometimes angular garnet fragments with dendritic overgrowths rim the injection veins. Such fragments form due to cataclasis of garnet porphyroclasts, dragging by melt and subsequent overgrowth by new dendritic rims (Pittarello et al. 2012).

Another feature characteristic for the pseudotachylytes are needle-shaped fine grains, ranging from 1 to 5 μm in length. Possibly these grains are locally preserved microlites, resulting from non-equilibrium crystallization of frictional melt (Appendix Figs. 2d and 2e).

In the sampled felsic mylonites, a fraction of 23-29% of all zircon grains are brittlely deformed, whereas 10-11% of all zircon grains show crystal-plastic deformation. These values are close to those for non-foliated metapelites sampled in the same area yielding about 24% brittlely and 11% crystal-plastically deformed grains, respectively. The content of deformed zircon grains in pseudotachylytes and in associated ultramylonites is much higher. There, 63-72% of grains are brittlely deformed (Fig. 8) and 19-28% show crystal-plastic deformation (Fig. 7), including grains with planar deformation bands (Figs. 1-4).